Conference paper

Benedetta Maria Squeo, Francesco Carulli, Elisa Lassi, Francesco Galeotti, Umberto Giovanella, Silvia Luzzati and Mariacecilia Pasini*

Benzothiadiazole-based conjugated polyelectrolytes for interfacial engineering in optoelectronic devices

https://doi.org/10.1515/pac-2018-0925

Abstract: Polar semiconducting polymers based on a conjugated polymer backbone endowed with chemically anchored polar groups on the side chains have proved to be particularly interesting as optimization layer at organic/cathode interface in optoelectronic devices. In particular, the pendant phosphonate groups impart water-alcohol solubility allowing easy solution processing, and improve electron injection thanks to both a favorable interfacial dipole of phosphonate groups and an intense coordination interaction between the phosphonate groups and Al cathode. In this work we synthesize alternating fluorene-benzothiadiazole copolymers by proposing a post-polymerization reaction to insert the phosphonate groups. Thanks to this approach it is possible to use standard Suzuki coupling conditions, simplifying the process of synthesis, purification and characterization. The polymer Poly[9,9-bis(6′-diethoxylphosphorylhexyl)-alt-benzothiadiazole] (P2), is tested in conventional organic solar cells as cathode interfacial layers showing, with respect to the control device, an increasing of all the photovoltaic parameters, with a final power conversion efficiency that reaches 5.35 % starting from 4.6 %. The same trend is observed for multilayered polymer light-emitting diodes with an external quantum efficiency of the P2-based PLED enhanced of 1.5 times with respect to the basic devices with bare Al cathode, and negligible roll-off efficiency. The synergic effects of energy gap modulation and of polar phosphonated pendant functionalities of P2 are compared with the corresponding fluorene-based polar homopolymer. Our results show that, not only a proper selection of side functionalities, but also the tailoring of the energy gap of cathode interfacial materials (CIMs) is a possible effective strategy to engineer cathode of different optoelectronic devices and enhance their performance.

Keywords: conjugated polymers; interfacial engineering; optoelectronics; POC-2018; polyelectrolytes.

Introduction

During the last decade, solution processable optoelectronic devices based on organic semiconducting materials have attracted great interest because they are the basis for the development of low-cost electronics. In particular organic light-emitting diodes (OLEDs) and organic solar cells (OSCs) are the most investigated

Article note: A collection of papers presented at the 17th Polymers and Organic Chemistry (POC-2018) conference held 4–7 June 2018 in Le Corum, Montpelier, France.

***Corresponding author: Mariacecilia Pasini,** Istituto per lo Studio delle Macromolecole Consiglio Nazionale delle Ricerche, Milano, Italy, e-mail: pasini@ismac.cnr.it. https://orcid.org/0000-0002-7811-6367
Benedetta Maria Squeo, Francesco Carulli, Elisa Lassi, Francesco Galeotti, Umberto Giovanella and Silvia Luzzati: Istituto per lo Studio delle Macromolecole Consiglio Nazionale delle Ricerche, Milano, Italy. https://orcid.org/0000-0002-5260-512X (B.M. Squeo); https://orcid.org/0000-0002-8345-6606 (F. Carulli); https://orcid.org/0000-0003-4793-9827 (F. Galeotti); https://orcid.org/0000-0003-2865-050X (U. Giovanella); https://orcid.org/0000-0001-7982-2215 (S. Luzzati)

devices, thanks to their appealing advantages like flexibility, lightness, transparency and possibility for roll-to-roll or ink-jet printing [1–7].

Interfacial engineering has been shown to play a fundamental role in the development of organic optoelectronics. In fact, current optoelectronic devices, regardless of the type of application (lighting, photovoltaics, sensors, etc.), are composed of organic multilayer systems and metal electrodes. In those type of architectures, it is fundamental the control of the quality of the interfaces in order to optimize the performance of the devices [8–11].

In recent years it has been demonstrated how the optimization of the interface between the metal electrode and the organic layer can be carried out by polar semiconductor polymers, also known as conjugated polyelectrolytes (CPEs). The structure of CPEs is typically composed by a π conjugated backbone endowed with polar pendant groups such as ammonium cationic groups [12, 13], sulfonate anionic groups [14, 15], and/or polar groups like phosphonate or amino functionalities [16] able to guarantee the solubility in environment-friendly water or alcohol solvents [17]. Moreover, the solubility in an orthogonal solvent with respect to the active layer solubility, allows for the fabrication of solution processed multilayer structure up to now peculiarity of a vacuum growth devices.

CPEs combine the typical characteristics of semiconducting polymers such as low-cost, flexibility, lightness, transparency, modulability, and organic films affinity with that of polar systems such as solubility in aqueous solvents, high dipole moments and strong interaction with the metal electrode.

Generally, the CPEs used at the interface with the cathode (also called cathode interfacial modifiers or CIMs) are based on a polyfluorene backbone bearing cationic, anionic or polar groups at the end of the lateral alkyl chains. Although the operating mechanism is not yet fully elucidated, it has been proposed that it origins from the charged or polar groups on the side chains, which can generate positive interfacial dipole between the electrode and the active layer, and from the interactions between the metal electrode and polar groups [18].

CPEs can be synthesized by following two different approaches. In the first case, the monomer is functionalized and subsequently polymerized, generally through a Suzuki coupling. Even though this synthetic route ensures a complete control of the degree of functionalization of the monomer, it requires the optimization of the polymerization conditions for each reaction because of the variations in the reactivity of the monomer. The most important CPEs synthesized in this way are those with amino [19], sulfonate [20] and phosphonate groups [21]. The second approach consists in the synthesis of a polymer having the lateral alkyl chains with brominated end groups which allow to make a post-polymerization functionalization [22]. The main advantage relies on the use of standard polymerization conditions with characterizations and purifications performed with traditional methods. Common polymers synthesized with a post-polymerization functionalization are those containing the ammonium group [23, 24]. Even if a limiting factor of this approach is the possible incomplete replacement of all the lateral substituents, we recently showed that by applying post-polymerization functionalization on phosphonate polymers with fluorene-based conjugated backbone, a nearly complete phosphonation can be achieved [25].

Previously, it has been reported that pendant phosphonate moieties in conjugated polymers can impart solubility in environmental-friendly alcohol solutions (e.g. ethanol) without affecting the electronic structure of conjugated polymer backbone [26, 27]. Meanwhile, the neutral character of these polymers eliminates the concern of mobile ions in the device, therefore enhancing lifetime of devices [28].

It was reported that in conventional P3HT:$PC_{60}BM$ based solar cells with conjugated poly[9,9-bis(6′-diethoxylphosphorylhexyl)fluorene] (PF-EP) as cathode buffer layer, the incorporation of 5 nm PF-EP can lead to improved open circuit voltage (V_{OC}) and fill factor (FF), and hence result in almost a two fold increase of PCE [29].

Similarly, multilayered OLEDs integrating PF-EP as Al CIM exhibit higher performance compared to the control device with Ca/Al cathode. The performance enhancement was attributed to the efficient electron injection caused by both a favorable interfacial dipole and intense coordination ability of phosphonate groups at the PF-EP/Al interfaces [30]. More importantly, in that solution-processed multilayered structure, the metal atoms diffusion into the emissive layer and exciton quenching at the cathode interface were prevent [31].

Although the possibility of tuning the conjugated backbone is one of the main advantages of organic semiconducting polymers, this issue has been rarely studied and exploited so far in the case of polar non-ionic CPEs.

The modification of the polymer backbone, and hence the tuning of the energy gap, in the CIM should affects energy barriers for electron injection at the interface with the cathode.

In this context, we synthesized a CPE having as conjugated backbone an alternating copolymer based on fluorene and benzothiadiazole bearing the phosphonated moieties as side polar groups, obtained through a post-polymerization reaction. Through a complete chemical characterization, we have shown that it is possible to obtain an almost complete post-polymerization functionalization with phosphonate moieties. The obtained CPE, soluble in orthogonal solvents with respect the active layer, was deposited from solution at the interface with the cathode and tested in conventional OPV showing an increasing of all the photovoltaic parameters with respect to the control device, with a final PCE that reaches 5.35 % starting from 4.6 %. The same trend is observed in conventional OLED with an external quantum efficiency that is enhanced of 1.4 times with respect to the control device with bare Al cathode.

These improvements were attributed both to phosphonate functionalities and main backbone energy gap modulation of the CIM.

Experimental

Materials

All reagents, included 2,7-Dibromo-9,9-bis(6-bromohexyl)fluorene and 2,1,3-Benzothiadiazole-4,7-bis(boronic acid pinacol ester) were purchased from commercial source and used without further purification. Toluene was freshly distilled prior to use according to literature procedure. All reactions were carried out in inert atmosphere. PTB7 was purchased from 1-Materials, $PC_{71}BM$ from Solenne, PEDOT:PSS Clevios (VP Al 4083) from Heraeus.

Synthesis of polymer P1 (Poly[9,9-bis(6′-dibromohexyl)-alt-benzothiadiazole])

A mixture of 2,7-Dibromo-9,9-bis(6-bromohexyl)fluorene, 2,1,3-Benzothiadiazole-4,7-bis(boronic acid pinacol ester), Tetrakis(triphenylphosphine)palladium(0) [$Pd(PPh_3)_4$], tetrabutylammonium bromide (TEBAB) were added in a pre-degassed schlenk, followed by three vacuum/nitrogen cycles. Then dry toluene and degassed potassium carbonate aqueous solution were added. The mixture was stirred at 110 °C. After 3 h, bromobenzene was added for capping the polymer and 12 h later phenyl boronic acid was added. The reaction mixture was filtered through a pad of celite and the solvent removed at reduced pressure. The crude was then redissolved in toluene and precipitated in methanol. The polymer was obtained as yellow solid with a yield of 75 %. ^{1}H NMR (600 MHz, $CDCl_3$): δ 8.0–7.4 (m, 8 H, Ar-H), 3.3 (m, 4 H, CH_2-Br), 2.2–2.0 (m, 4 H, aliphatic chain), 1.7 (m, 4 H, aliphatic chain), 1.3–1.1 (m, 8 H, aliphatic chain), 0.9–0.7 (m, 4H, aliphatic chain). SEC (THF, polystyrene standard) analysis showed an $M_w = 10\,000$ and PDI = 2.4.

Synthesis of polymer P2 (Poly[9,9-bis(6′-diethoxylphosphorylhexyl)-alt-benzothiadiazole])

Polymer 1 and triethyl phosphite were added in a pre-degassed schlenk and the mixture was stirred at 140 °C overnight. Then the excess of triethyl phosphite was removed at reduced pressure. Polymer P2 was obtained as gummy yellow solid in quantitative yield. ^{1}H NMR (600 MHz, $CDCl_3$): δ 8.0–7.91 (m, 8 H, Ar-H), 4.0 (m, 8 H, P-O-CH_2), 2.2 (m, 4 H, aliphatic chain), 1.62 (m, 8 H, aliphatic chain), 1.48 (m, 4 H, aliphatic chain), 1.26 (m, 12 H, -O-CH_2-CH_3), 1.18 (4 H, aliphatic chain), 0.9 (m, 4 H, aliphatic chain).

Devices fabrication and characterization

Solar cells were assembled with the conventional structure Glass/ITO/PEDOT:PSS/PTB7:PC71BM/interlayer/Al. Glass ITO (Kintec) 15 Ω/sq substrates were mechanically cleaned with peeling tape and paper with acetone and then were washed in a sonic bath at 50 °C for 10 min sequentially with water, acetone, and isopropanol. After drying with compressed nitrogen flow, 10 min plasma treatment in the air was used to enhance ITO wettability for the next deposition. PEDOT:PSS was filtered on a 0.45 μm nylon filter, spin-coated in the air at 2500 rpm for 50 s and finally stored in a glovebox and annealed at 110 °C for 10 min. The device assembly was then performed in glovebox. The active layer was composed by a blend of 1:1.5 wt/wt of PTB7:PC71BM dissolved in 1-chlorobenzene at a total concentration of 23 mg/ml. The solution was stirred for 12 h on a hotplate in glovebox at 60 °C; subsequently, a 1.8 % v/v of 4-anisaldehyde was added to the blend solution 15 min prior to deposition. In PTB7:PC71BM blends, 4-anisaldehyde was reported to be almost as effective as 1,8-diiodooctane additive, but its higher volatility ensures a better stability in time of the active layer morphology with no need of further washing step to remove additive residues [32]. The active layer was spin-coated from the warm solution at 1000 rpm for 60 s, which results in a thickness of 90 nm; then, the device was placed on a 65 °C hotplate for 15 min to help solvent evaporation. In the case of the devices containing the interlayer, 60 μl of ethanol solutions (at 1 mg/ml for P2 and 0.5 mg/ml for PF-EP) were dropped on the rotating device at 4000 rpm for 60 s, while in the case of ethanol-treated device, the same conditions were adopted for the surface washing with a pure ethanol solution. Finally, a 100 nm-thick aluminum electrode was evaporated on the top of the device through a shadow mask under a pressure of 2×10^{-6} mbar. The deposition rate was 0.5 nm/s. There were six devices on a single substrate, each with an active area of 6.1 mm^2.

OLEDs were assembled with the conventional structure Glass/ITO/PEDOT:PSS/poly(9,9-dioctylfluorene-*alt*-benzothiadiazole) (or F8BT)/interlayer/Al. The glass ITO 15 ohm/sq (Kintec) was cleaned by following the procedure reported for solar cells. A 40 nm-thick PEDOT:PSS layer was spin-coated and consequently annealed at 150 °C for 10 min inside a nitrogen-filled glovebox. The emitting layer is composed by commercially available F8BT (American Dye Source). F8BT layer is prepared in glovebox by spin-coating a 15 mg/ml toluene solution at 2000 rpm. Polar polymers are spin-coated from a 5 mg/ml EtOH solution at 4000 rpm. Aluminum cathode (100 nm) is finally evaporated on top of the organic layers as reported above. There were four devices on a single substrate, each with an active area of 6.8 mm^2.

Current density-voltage measurements on solar cells were performed directly in the glovebox where the solar cells were assembled, with a Keithley 2602 source meter, under dark or under an AM 1.5 G solar simulator (ABET 2000). The incident power, measured with a calibrated photodiode (Si cell + KG5 filter), was 100 mW/cm^2. The EQE spectral responses were recorded by dispersing an Xe lamp through a monochromator, using a Si solar cell with a calibrated spectral response to measure the incident light power intensity at each wavelength. The devices were taken outside the glovebox for the EQE measurements, after mounting them on a sealed cell to avoid moisture and oxygen exposure. Current density-luminance-voltage measurements of OLEDs were performed in the glovebox with a Keithley 2602 source meter and Konica-Minolta LS-150. Electroluminescence spectra were recorded by means of Ocean optics USB4000 spectrometer.

Results and discussion

Synthesis and chemical characterization

The chemical structure of the polymers is shown in Fig. 1.

Polymer P1 was synthesized through Suzuki cross coupling of an alkyl bromide-substituted fluorene and the bis-boronic ester of benzothiadiazole, with $Pd(PPh_3)_4$ as catalyst and K_2CO_3 as base (Fig. 2a). P2 was obtained by refluxing P1 in excess of triethyl phosphite (Fig. 2b) for 24 h at 140 °C after complete dissolution of P1.

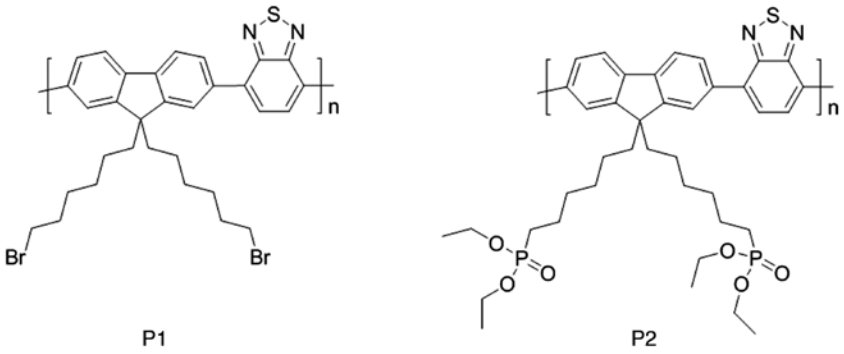

Fig. 1: Chemical structures of polymers P1 and P2.

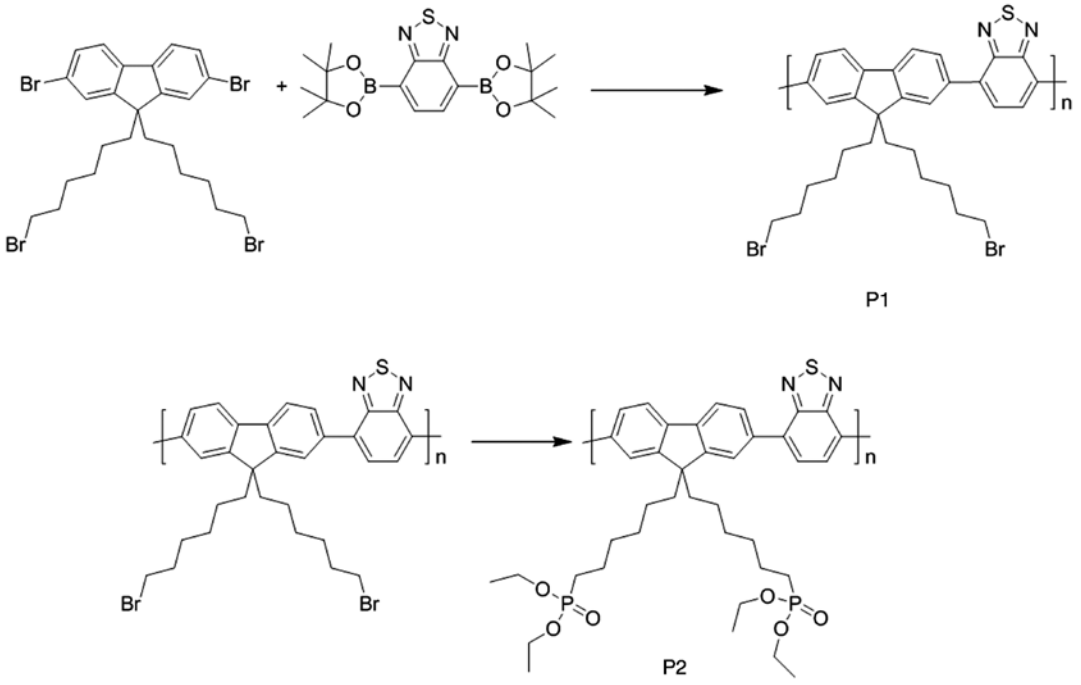

Fig. 2: Synthesis of polymers P1 (a) and P2 (b).

Differently from other phosphonated materials where the functionalization was performed on the monomer, we decide to use a post polymerization approach. This kind of functionalization has the advantage to obtain a soluble polymer in organic solvents by common cross coupling polymerization, like Suzuki coupling, that can be easily characterized by GPC and NMR technique before substitution, while the main drawback could be the non-quantitative functionalization.

The chemical structure of polymer P1 and P2 have been characterized with ^{1}H and ^{31}P NMR and FTIR to evaluate the degree of substitution, the molecular weight has been determined by size exclusion chromatography (SEC) and their thermal decomposition temperatures were studied by thermo-gravimetric analysis (TGA).

The comparison between the NMR spectra of P1 and P2 shows the complete disappearing of the CH2-Br group at 3.3 ppm and the appearance of new signals due to the ethyl group of phosphonate at 4.1 ppm and 1.2 ppm (Fig. 3).

The successful introduction of the phosphonate groups has been also confirmed by the ^{31}P NMR spectrum, showing only a signal at 33 ppm [26] originating from phosphonate groups (Fig. 3 inset).

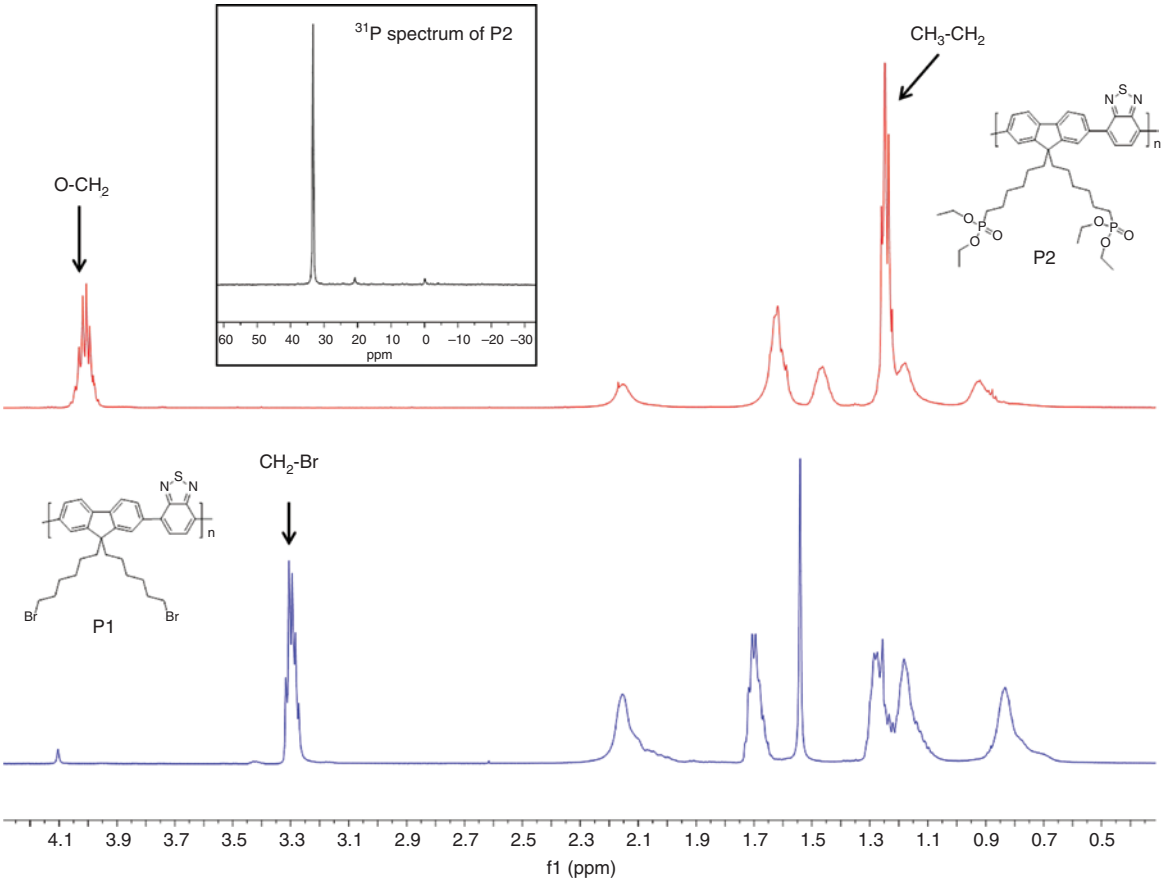

Fig. 3: H NMR spectra recorded in CDCl of P1 (blue) and P2 (red). P NMR spectrum recorded in CDCl of P2.

The FTIR spectrum (Fig. 4) of P2 confirms the presence of phosphonate moieties and shows rocking vibration bands of P–O–Et between 950 and 1090 cm^{-1} and P=O stretching at 1230 cm^{-1}, demonstrating the successful phosphonation of polymer P1, confirmed also by the disappearing of the C–Br stretching at 643 cm^{-1}.

The thermogravimetric analysis of both the polymers P1 and P2 show three steps degradation (Fig. 5a), compatible with the sequential degradation of the pending groups (Br in case of P1 and phosphonate in case of P2) at 345 °C and 360 °C for P1 and P2, respectively, of the long hexyl chain at 490 °C and 515 °C and then the main chain decomposition.

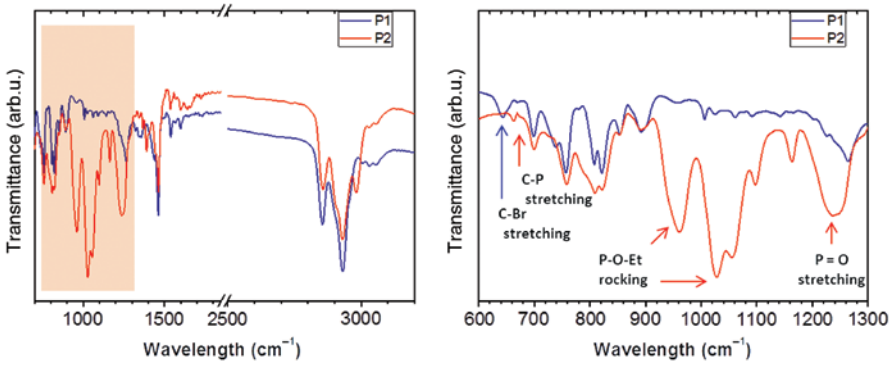

Fig. 4: FTIR spectra of polymers P1 (blue line) and P2 (red line).

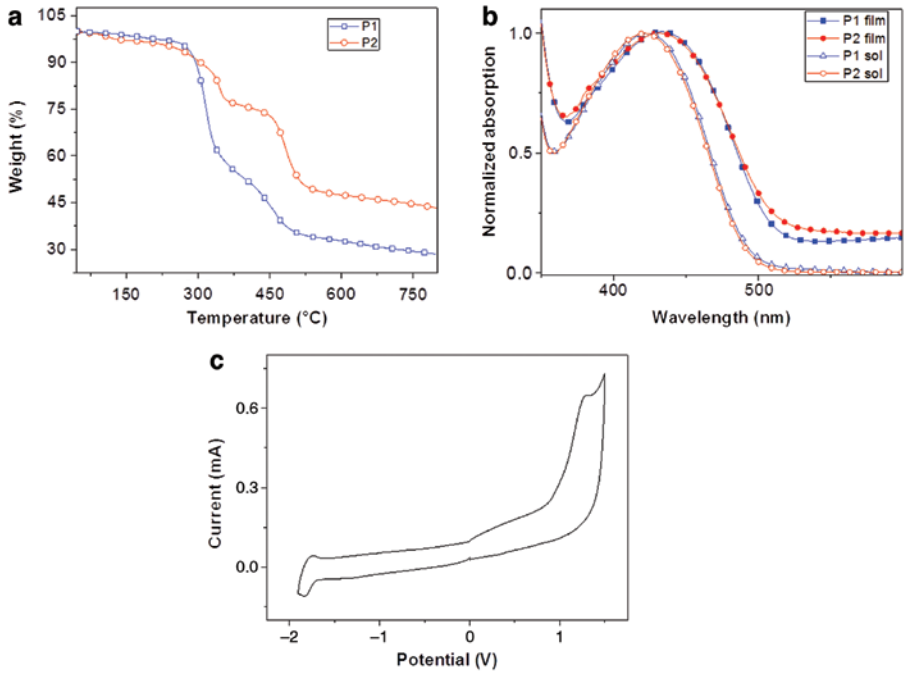

Fig. 5: (a) Thermo-gravimetric curves of P1 and P2 at a heating rate of 10 °C/min. (b) Normalized absorption spectra in chloroform solution and film of P1 and P2. (c) Cyclic voltammogram of P2 in 0.1 M n-Bu NClO; scan rate: 100 mVs.

As previously reported by Wang et al. [21], the pendant phosphonate moiety can make conjugated polymers soluble in polar organic solvents (e.g. ethanol) without affecting the electronic structure of the polymer backbone, as confirmed by the absorption spectra of polymer P1 and P2 in Fig. 5b.

Cyclic voltammetry has been applied to investigate the electrochemical properties. A glassy carbon, coated with P2 was used as the working electrode and a solution of tetra-n-butylammonium perchlorate (0.1 M Bu_4NClO_4) in anhydrous acetonitrile was used as the electrolyte.

The onset oxidation potential of P2 is located at 0.97 eV whereas the reduction potential is situated at –1.72 eV (Fig. 5c). The highest occupied molecular orbital (HOMO) and lowest unoccupied molecular orbital (LUMO) levels were estimated by using the equations $E_{HOMO} = -(E_{ox} + 4.39 + 0.34)$ eV and $E_{LUMO} = -(E_{red} + 4.39 + 0.34)$ eV [33], where E_{ox} and E_{red} are the onset reduction and oxidation potentials, respectively, relative to the vacuum scale. The HOMO and LUMO energy levels P2 are –5.8 eV and –3.01 eV, respectively.

PF-EP shows HOMO and LUMO leveles located at –5.7 eV and –2.2 eV [25], respectively. The downshift of the LUMO level of P2 compared to PF-EP is due to the presence of benzothiadiazole unit.

Devices

By following the idea of testing F8BT-EP as an interfacial layer in optoelectronic devices, we have prepared and characterized OSC and OLED prototypes with a conventional geometry (Figs. 6d and 7d). A PF-EP CIM [25] was included in this study to get insights about the effect of the backbone modification on the devices performances. CIM films were deposited by spin-coating from ethanol solutions on top of the active layers with thickness optimized for the different devices.

Organic solar cells

For solar cells the optimal thickness of the interlayer was found to be around 5–10 nm [18, 34]. To evaluate the interfacial modification capability of these two polymers, we added to the comparison untreated devices

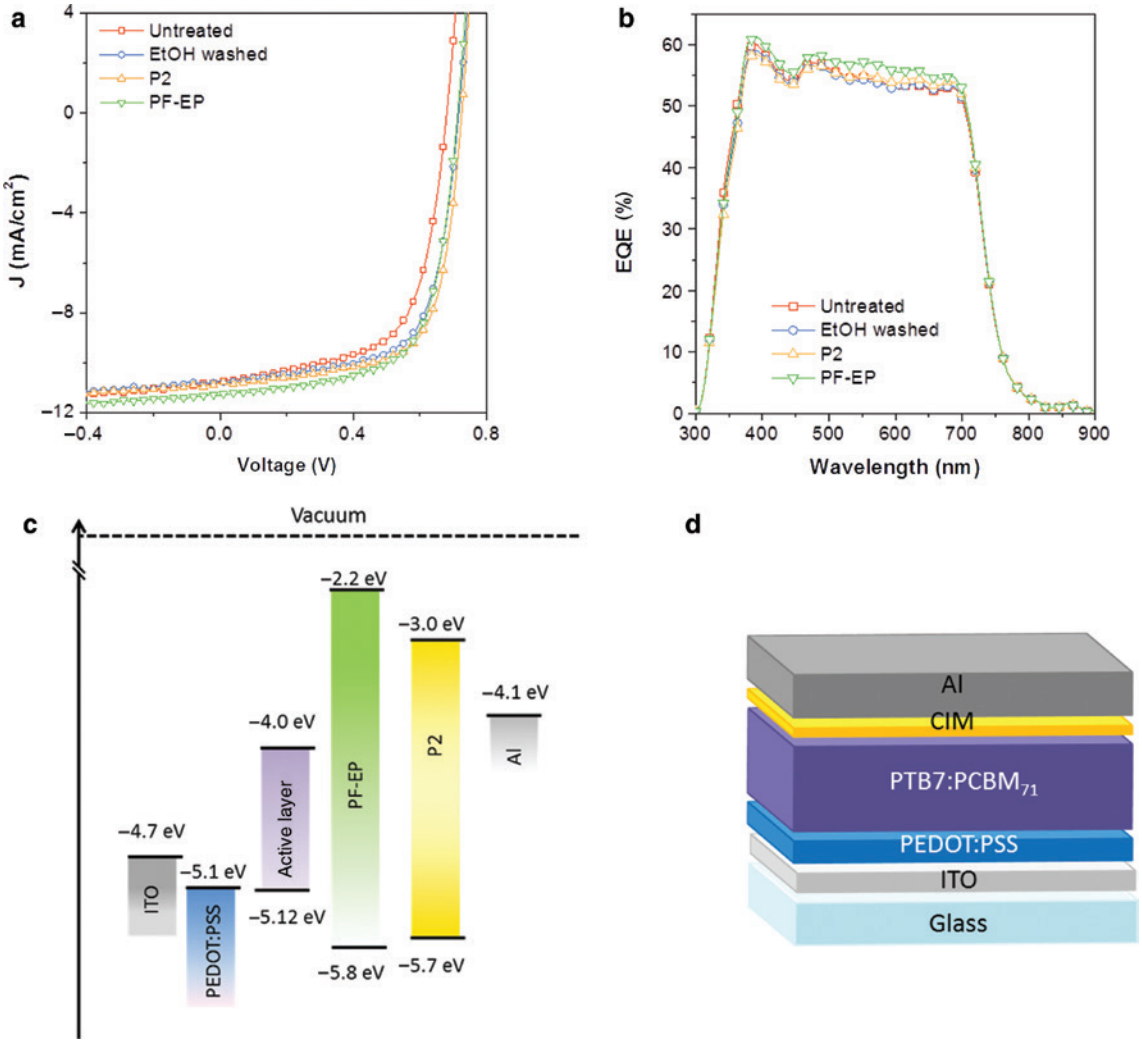

Fig. 6: (a) Current-voltage plot of an untreated device, ethanol treated device, device containing P2 polymer and PF-EP polymer. (b) External quantum efficiency plots of the same set of devices. (c) Energy levels diagram. (d) Structure of the OSC device with interlayer.

without any interlayer, where the Al electrode was directly evaporated on top of the active layer (pristine Al). To distinguish the effect induced by the polymeric interlayers from the effect of the alcohol solvent used for their deposition we added to this comparison a device without the interlayers, which was treated with bare ethanol before the Al evaporation (EtOH).

The J-V characteristics and EQE spectra of the devices are shown in Fig. 6a and b while the corresponding photovoltaic parameters estimated from the J-V curves are summarized in Table 1, together with the devices series and shunt resistances. The untreated device exhibits a typical PCE of 4.6 %. Ethanol treatment rises the PCE to 5.13 %, due to an increase of the V_{OC} (from 0.68 to 0.71) and an enhancement in the FF (from 0.627 to 0.663), combined to a lower series resistance and higher shunt resistance. Such results are consistent with what has been reported in the literature about surface alcohol treatments on the active layer. The increased FF and V_{OC} upon alcohol treatment were reported to be due to an enhancement of the V built-in across the device, mostly related to the modification of the buried PEDOT:PSS/active layer interface, leading to better hole extraction and increased selectivity of the contacts [35].

The device containing P2 shows a higher FF (0.677) and V_{OC} (0.73), which can be explained considering the modification effect of high-polarity materials, such as P2, on the metal cathode. The WF of the cathode is shifted towards the vacuum level because of the polarity of the interlayer [34–36], which results in increased

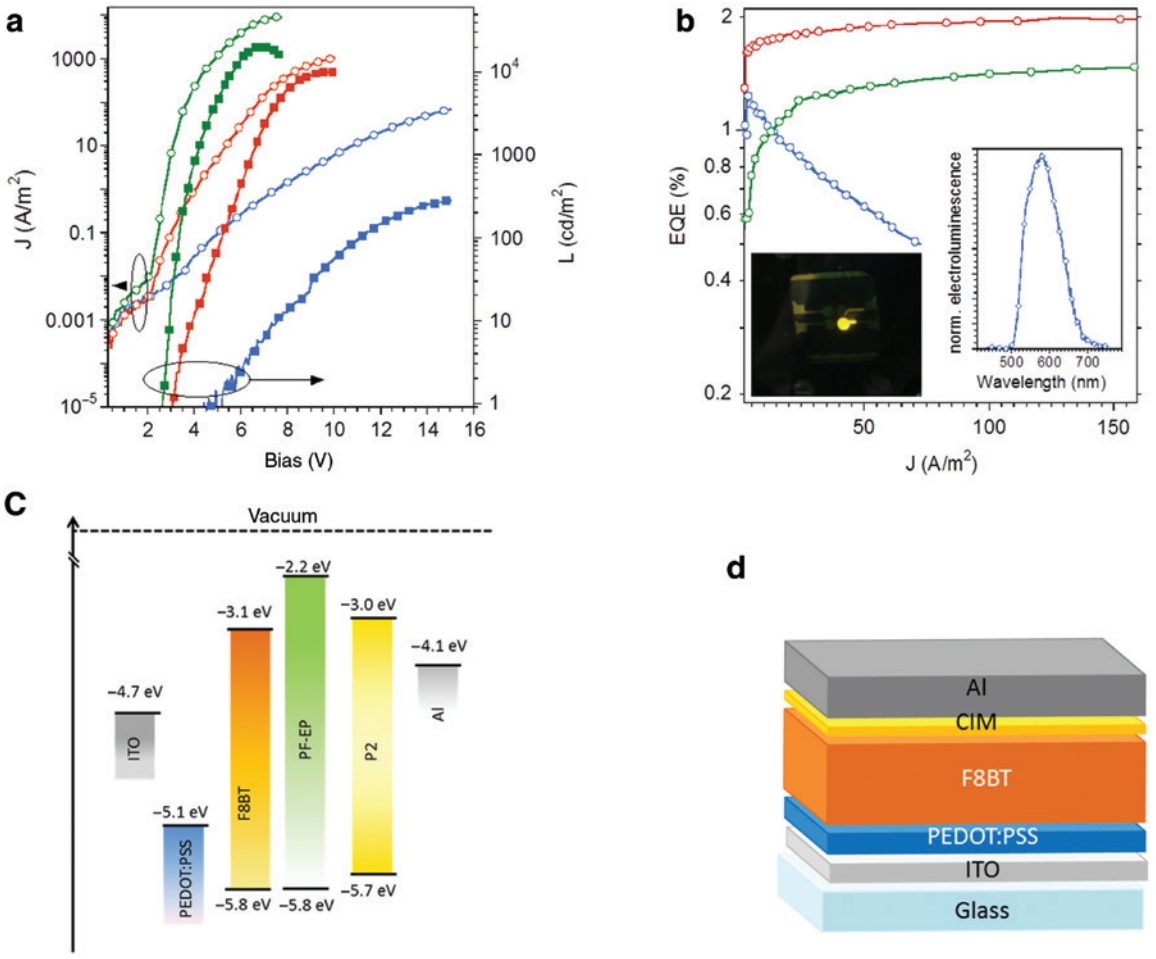

Fig. 7: (a) EL spectra of basic ITO/PEDOT:PSS/F8BT/Al (blue line), ITO/PEDOT:PSS/F8BT/P2/Al (red line) and ITO/PEDOT:PSS/F8BT/PF-EP/Al (green line) devices and (b) corresponding EQE vs. current density (in the inset, picture of turned on ITO/PEDOT:PSS/F8BT/P2/Al device and representative EL spectrum). (c) Energy levels diagram [39]. (d) Structure of the OLED device with interlayer.

anode-cathode band offset, revealed by an enhanced V_{OC}. The aluminum WF shift is beneficial also for what concerns the energy-level alignment with the electronic level of the active layer. The modified-level alignment at the interfaces improves the extraction of electrons from the device.

As a result, the series resistance decreases while the shunt resistance is enhanced compared to ethanol treated device. Similar features are also observed when using a PF-EP cathode interlayer. Table 1 highlights that while the PCE of the device prepared with PF-EP is only slightly lower than the one obtained with P2 (5.32 % instead of 5.35 %), the other PV parameters reveal some differences between the two CIMs. P2 based devices show higher Voc, FF and lower series resistance compared to PF-EP. On the other side PF-EP devices show a higher J_{sc} and a slightly higher shunt resistance. Such behavior can be tentatively explained considering the electronic properties of the two polymeric compounds.

The higher electronic affinity of P2 favors electron extraction to the cathode, thus reducing series resistance and enhancing FF. The V_{oc} is likely higher than in PF-EP as the better electron extraction is reducing charge recombination which is a limiting factor for the V_{oc} parameter [37]. The PF-EP CIM is likely a better hole blocking material than P2 due to its slightly lower HOMO energy level and this is consistent with a slightly higher shunt resistance observed for PF-EP devices. It was reported [38] that PF based CIMs thin layers of few nanometers could act as optical spacers, inducing an enhancement of the J_{sc}. We suggest that a similar feature can explain the enhancement of the J_{sc} observed in PF-EP devices. P2, with its lower optical energy gap, is less effective in engineering the absorbed photons in the device than PF-EP, leading thus to a lower J_{sc}.

Table 1: Photovoltaics parameters of devices with different cathode (average values of 12 devices).

	Voc (V)	FF	Jsc (mA/cm^2)	PCE (%)	Rsh (kΩ*cm^2)	Rs (Ω*cm^2)
Al_{un}	0.68 ± 0.01	0.627 ± 0.003	10.8 ± 0.5	4.6 ± 0.3	500 ± 30	6.4 ± 0.3
$Al_{EtOH\ wash}$	0.71 ± 0.01	0.65 ± 0.05	10.7 ± 0.3	5.0 ± 0.4	1490 ± 70	6.3 ± 0.3
P2/Al	0.73 ± 0.01	0.677 ± 0.009	10.8 ± 0.5	5.3 ± 0.2	2310 ± 120	5.0 ± 0.2
PF-EP/Al	0.71 ± 0.01	0.663 ± 0.004	11.3 ± 0.8	5.3 ± 0.4	2950 ± 170	5.7 ± 0.2

In conclusion, P2, thanks to its phosphonate polar groups, is effective in engineering the interface among the active layer and the Al cathode when used in OSCs, enhancing the electron extraction and contact selectivity. The comparison of the OSC devices featuring P2 as CIM with the corresponding phosphonated polymers based on polyfluorene backbone, PF-EP, shows that PV parameters nicely correlate with the electronic properties of CIMs.

Polymer light-emitting diodes (PLEDs)

The performance of PLEDs can be boosted by integrating proper polar polymers as a thin CIM layer at the cathode interface. The suitable choice of the CIM can even allows the substitution of the highly reactive Ca or Ba layer, normally employed to facilitate electron injection into the emissive layer and deposited only by thermal evaporation.

PLED architecture ITO/PEDOT:PSS/F8BT/CIM/Al with the two different CIMs and the control device ITO/PEDOT:PSS/F8BT/Al, featuring bare Al cathode, have been fabricated and characterized.

The performance of F8BT-based PLEDs with bare Al cathode are poor due to both limited injection of electrons from Al cathode into the LUMO level of F8BT (see Fig. 7c) and the exciton-quenching at cathode interface [40].

The CIM layer is deposited on top of the emitting layer and covered by the Al cathode. The thickness of the CIM layer is critical and was intentionally fixed around 20 nm for PF-EP and P2 interlayers as it is reported to be the optimized value in OLEDs [19].

The reduction of cathode's |WF| induced by the presence of the CIMs layer, as observed for OPV and due to the formation of an interface dipole [41], is beneficial for electrons injection into the active layer. As a consequence, a large reduction of turn on voltage (V_{ON}), of more than 2 eV, is achieved in the CIM-based devices (Fig. 7a) with an enhancement of external quantum efficiency (EQE) from 1.26 % in the basic architecture, to 1.59 and 2.01 % for PF-EP and P2-based OLEDs, respectively (Fig. 7b).

The engineered cathode, with the insertion of CIM layer that in addition exploited the affinity between phosphonate polar groups and the metal [30], resulted in stronger luminance (L = 20 703 and 10 107 cd/m^2 for PF-EP and P2-based devices, respectively) with respect to the basic architecture (L = 286 cd/m^2) (Fig. 7a). Electroluminescence spectra of three devices show typical features of F8BT emission (inset of Fig. 7d).

The thickness of CIM layer integrated in the current PLEDs is larger than in the case of OSC. Therefore, the effect on electron injection barrier could be ascribed not only to the formation of an interfacial dipole, but also to a combination of a reorientation of the ionic side chains under a given electric field [18] and the LUMO energy level of the bulk polar polymers film, i.e. the different polymer backbone since functional lateral groups are the same in both CIMs.

The electron injection properties and efficiency of the F8BT-based PLEDs using CIMs are comparable or better than those of basic devices containing Ba/Al composed cathode [42].

The basic device, with bare Al cathode, suffers from a severe roll-off efficiency most probably due to a quenching of radiative recombination at the polymer/cathode interface. The insertion of CIM, besides a mitigation of energy barrier for electron injection, confines the recombination zone of radiative excitons within the F8BT layer and far from the cathode, resulting in a negligible roll-off efficiency (Fig. 7b). The EQE of

Table 2: Main PLEDs performance details.

	V_{ON} (V)[a]	EQE_{MAX} (%)	LE_{MAX} (cd/A)[b]	L_{MAX} (cd/m²)
Basic	5.0	1.26 (1.01 ± 0.25)[c]	/	286
PF-EP	2.7	1.59 (1.50 ± 0.12)[c]	3.67	20 703
F8BT-EP	3.0	2.01 (1.97 ± 0.06)[c]	5.69	10 107

[a]1 cd/m².
[b]1000 cd/m².
[c]Average values of eight devices.

CIM-based devices remains above 1 % in the large range of L from 1 to 10 000 cd/m². Since the HOMO energy levels of F8BT and CIMs are similar, negligible hole blocking role of CIMs can be envisaged. In Table 2 main PLEDs performance are gathered.

Conclusions

Poly[9,9-bis(6′-diethoxylphosphorylhexyl)-alt-benzothiadiazole] P2 was synthesized via post-polymerization functionalization with triethyl phosphite of the corresponding brominated polymer obtained via standard Suzuki coupling. The complete phosphonate substitution was confirmed via 1H and 31 P NMR.

Thanks to the P2 solubility in alcohol, solvent that is orthogonal to the solubility of the active layer the CIM was successfully applied as cathode interfacial layer in both PLEDs and OSCs.

In the OSC prototypes, if compared to the control device, we observe an enhancement of all the photovoltaic parameters, with a final PCE that reaches 5.35 % starting from 4.6. Such effect is mostly due to the phosphonate polar groups, which are effective in engineering the interface among the active layer and the Al cathode, enhancing the electron extraction and contact selectivity. The phosphonate polyfluorene interlayer PF-EP device shows a PCE similar to P2-based OSC, but suggests that the conjugated backbone also influences the photovoltaic characteristics through a delicate balance between the energy level alignment with electronic level of the active layer and its hole blocking behavior.

The favorable interfacial dipoles of phosphonate groups together with an intense coordination interaction between the phosphonate groups and Al at CIM/Al interface are mainly responsible for the efficient electron injection in PLEDs. As a result, the devices with CIM engineered cathode demonstrate superior performance compared to the devices with Al, and even Ba/Al, cathode due to efficient electron injection and suppressed exciton-quenching at cathode interface. The device with P2 exhibits of an efficiency 2 %, greater than the 1.5 % obtained with the corresponding phosphonate polyfluorene PF-EP and 1 % of the control device.

The proper selection of side functionalities, combined to the tailoring the energy gap of CIMs is a possible effective strategy to engineer cathode of different optoelectronic devices, like OLEDs and OPVs, and enhance their performance. We believe that the obtained knowledge in this work can contribute to advances in further developing high performance conjugated polar polymers for interfacial engineering.

Acknowledgments: The authors wish to thank Alberto Giacometti-Schieroni (ISMAC-CNR) for GPC and Dr. Fabio Bertini e Dr. Maurizio Villani (ISMAC-CNR) for thermal characterization and Dr. Barbara Vercelli (ICMATE-CNR) for Cyclic voltammetry.

References

[1] M. Kaltenbrunner, M. S. White, E. D. Głowacki, T. Sekitani, T. Someya, N. S. Sariciftci, S. Bauer. *Nat. Commun.* **3**, 770 (2012).
[2] R. Søndergaard, M. Hösel, D. Angmo, T. T. Larsen-Olsen, F. C. Krebs. *Mater. Today (Oxford, U. K.)* **15**, 36 (2012).

[3] S. Hollidaya, Y. Lia, C. K. Luscomb. *Prog. Polym. Sci.* **70**, 34 (2017).
[4] W. Zhao, S. Li, H. Yao, S. Zhang, Y. Zhang, B. Yang, J. Hou. *J. Am. Chem. Soc.* **139**, 7148 (2017).
[5] S. R. Forrest. *Nature* **428**, 911 (2004).
[6] K. T. Kamtekar, A. P. Monkman, M. R. Bryce. *Adv. Mater.* **22**, 572 (2010).
[7] U. Giovanella, M. Pasini, C. Botta. in *Applied Photochemistry*, G. Bergamini, S. Silvi (Eds.), pp. 145–196. Springer International Publishing, Switzerland (2016).
[8] X. Peng, L. Hu, F. Qin, Y. Zhou, P. K. Chu. *Adv. Mater. Interfaces* **5**, 1701404 (2018).
[9] R. Steim, F. R. Kogler, C. J. Brabec. *J. Mater. Chem.* **20**, 2499 (2010).
[10] H.-L. Yip, A. K. Y. Jen. *Energy Environ. Sci.* **5**, 5994 (2012).
[11] Z. Hu, K. Zhang, F. Huang, Y. Cao. *Chem. Comm.* **51**, 5572 (2015).
[12] F. Carulli, W. Mróz, E. Lassi, C. Sandionigi, B. Squeo, L. Meazza, G. Scavia, S. Luzzati, M. Pasini, U. Giovanella, F. Galeotti. *Chem. Pap.* **72**, 1753 (2018).
[13] M. Knaapila, T. Costa, V. M. Garamus, M. Kraft, M. Drechsler, U. Scherf, H. D. Burrows. *J. Phys. Chem. B* **119**, 3231 (2015).
[14] B. Xu, Z. Zheng, K. Zhao, J. Hou. *Adv. Mater.* **28**, 434 (2016).
[15] H. D. Burrows, V. M. M. Lobo, J. Pina, M. L. Ramos, J. Seixas de Melo, A. J. M. Valente, M. J. Tapia, S. Pradhan, U. Scherf. *Macromolecules* **37**, 7425 (2004).
[16] U. Giovanella, M. Pasini, M. Lorenzon, F. Galeotti, C. Lucchi, F. Meinardi, S. Luzzati, B. Dubertret, S. Brovelli. *Nano Lett.* **18**, 3441 (2018).
[17] C. C. Chueh, C. Z. Li, A. K. Y. Jen. *Energy Environ. Sci.* **8**, 1160 (2015).
[18] B. H. Lee, I. H. Jung, H. Y. Woo, H. K. Shim, G. Kim, K. Lee. *Adv. Funct. Mater.* **24**, 1100 (2014).
[19] A. Castelli, F. Meinardi, M. Pasini, F. Galeotti, V. Pinchetti, M. Lorenzon, L. Manna, I. Moreels, U. Giovanella, S. Brovelli. *Nano Lett.* **15**, 5455 (2015).
[20] C. K. Mai, H. Zhou, Y. Zhang, Z. B. Henson, T. Q. Nguyen, A. J. Heeger, G. C. Bazan. *Angew. Chem. Int. Ed.* **52**, 12874 (2013).
[21] B. Meng, Y. Fu, Z. Xie, J. Liu, L. Wang. *Polym. Chem.* **6**, 805 (2015).
[22] C. Chi, A. Mikhailovsky, G. C. Bazan. *J. Am. Chem. Soc.* **129**, 11134 (2007).
[23] R. Kang, S. H. Oh, D. Y. Kim. *ACS Appl. Mater. Interfaces* **6**, 6227 (2014).
[24] Z. B. Henson, Y. Zhang, T. Q. Nguyen, J. H. Seo, G. C. Bazan. *J. Am. Chem. Soc.* **135**, 4163 (2013).
[25] M. Prosa, E. Benvenuti, M. Pasini, U. Giovanella, M. Bolognesi, L. Meazza, F. Galeotti, M. Muccini, S. Toffanin. *ACS Appl. Mater. Interfaces* **10**, 25580 (2018).
[26] C.-S. Wu, C.-Y. Chou, Y. Chen. *J. Mater. Chem. C* **2**, 6665 (2014).
[27] B. Meng, Y. Fu, Z. Xie, J. Liu, L. Wang. *Macromolecules* **47**, 6246 (2014).
[28] F. Huang, Y. Zhang, M. S. Liu, A. K. Y. Jen. *Adv. Funct. Mater.* **19**, 2457 (2009).
[29] Y. Zhao, Z. Xie, C. Qin, Y. Qu, Y. Geng, L. Wang. *Sol. Energy Mater. Sol. Cells* **93**, 604 (2009).
[30] B. Zhang, C. Qin, X. Niu, Z. Xie, Y. Cheng, L. Wang, X. Li. *Appl. Phys. Lett.* **97**, 043506 (2010).
[31] B. Zhang, Z. Xie, L. Wang. *Polym. Bull.* **68**, 829 (2012).
[32] C. Sprau, F. Buss, M. Wagner, D. Landerer, M. Koppitz, A. Schulz, D. Bahro, W. Schabel, P. Scharfer, A. Colsmann. *Energy Environ. Sci.* **8**, 2744 (2015).
[33] M. D. Iosip, D. Destri, M. Pasini, W. Porzio, K. P. Pernstich, B. Batlogg. *Synth. Met.* **146**, 251 (2004).
[34] R. Xia, D.-S. Leem, T. Kirchartz, S. Spencer, C. Murphy, Z. He, H. Wu, S. Su, Y. Cao, J. S. Kim, J. C. deMello, D. D. C. Bradley, J. Nelson. *Adv. Energy Mat.* **3**, 718 (2013).
[35] Tan, Y. Vaynzof, D. Credgington, C. Li, M. T. L. Casford, A. Sepe, S. Huettner, M. Nikolka, F. Paulus, L. Yang, H. Sirringhaus, N. C. Greenham, R. H. Friend. *Adv. Funct. Mater.* **24**, 3051 (2014).
[36] H. Liu, L. Hu, F. Wu, L. Chen, Y. Chen. *ACS Appl. Mater. Interfaces* **15**, 9821 (2016).
[37] A. Kumar, G. Lakhawani, E. Elmalem, W. T. S. Huck, A. Rao, N. C. Greenham, R. H. Friend. *Energy Environ. Sci.* **7**, 2227 (2014).
[38] Y. Li, Y. Cheng, P. Yeh, S. Liao, S. Chen. *Adv. Funct. Mater.* **24**, 6811 (2014).
[39] J. Morgado, R. H. Friend, F. Cacialli. *Appl. Phys. Lett.* **80**, 2436 (2002).
[40] A. L. Burin, M. A. Ratner. *J. Phys. Chem. A* **104**, 4704 (2000).
[41] F. Huang, H. Wua, Y. Cao. *Chem. Soc. Rev.* **39**, 2500 (2010).
[42] V. Vohra, W. Mróz, S. Inaba, W. Porzio, U. Giovanella, F. Galeotti. *ACS Appl. Mater. Interfaces* **9**, 25434 (2017).

Graphical abstract

Benedetta Maria Squeo, Francesco Carulli, Elisa Lassi, Francesco Galeotti, Umberto Giovanella, Silvia Luzzati and Mariacecilia Pasini

Benzothiadiazole-based conjugated polyelectrolytes for interfacial engineering in optoelectronic devices

https://doi.org/10.1515/pac-2018-0925
Pure Appl. Chem. 2019; x(x): xxx–xxx

Conference paper: Pendant phosphonate groups in fluorene-benzothiadiazole-based conjugated polyelectrolytes impart water-alcohol solubility allowing easy solution processing, and improve electron injection thanks to both a favorable interfacial dipoles of phosphonate groups and an intense coordination interaction between the phosphonate groups and Al cathode. A proper selection of side functionalities, but also the tailoring of the energy gap of cathode interfacial materials is a possible effective strategy to engineer cathode of different optoelectronic devices and enhance their performance.

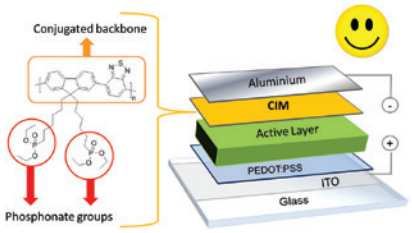

Keywords: conjugated polymers; interfacial engineering; optoelectronics; POC-2018; polyelectrolytes.